ANALYSIS OF PARAMETERS AND RESULTS FOR ON-THE-JOB CALIBRATION OF TERRESTRIAL LASER SCANNERS

Gábor Molnár (1), Camillo Ressl (2), Norbert Pfeifer (2), Peter Dorninger (1)
1. Christian Doppler Laboratory for "Spatial Data from Laser Scanning and Remote Sensing" at the Institute of Photogrammetry and Remote Sensing, Vienna University of Technology, A-1040 Vienna, Gußhausstraße 27-29.
2. Institute of Photogrammetry and Remote Sensing, Vienna University of Technology, A-1040 Vienna, Gußhausstraße 27-29.

gmo@ipf.tuwien.ac.at, car@ipf.tuwien.ac.at, pdo@ipf.tuwien.ac.at, np@ipf.tuwien.ac.at

Abstract: In this paper we present an on-the-job scanner calibration method. The basic concept of this method is that the measured points from different scanner positions should fit on planar object patches. Formulating this criterion in an adjustment process we estimate the range and angle measurement correction functions, the exterior orientation of the scanners and the parameters of the plane patches. The effect of the formulation of the correction function and the effect of patch size on the results is shown for an example in an interior room. We demonstrate that an improvement of the original status of the data is possible. The RMS of the normal distances of the points of the scans to the adjusted patches decreased from 1.7mm to 1.2mm.

1. Introduction

Measurements from a terrestrial laser scanner (TLS) are affected by systematic errors as it has been shown by different groups [1,2,3,4]. Random and systematic errors become smaller with new generations of instruments, but – even after a laboratory calibration of the scanner – systematic errors remain notable in the data acquired for a certain project. This may be attributed to an instability of the parameters determined during the laboratory calibration, or to a still limited understanding of the error sources. To minimize the remaining systematic errors in the project data an on-the-job calibration of the TLS is one possible solution. In this case the original TLS measurements are corrected by suitable functions, whose parameters are derived from the project data.

Previous investigations by different authors [2,5,6,7] found mainly two types of remaining systematic errors in the data (especially for the range measurements): periodic and non-periodic errors. For the periodic errors different dominating wavelengths were reported. In this work we investigate the improvement of the geometric quality of TLS data by on-the-job calibration using correction function, which are a sum of different periodic functions and a piecewise linear function. For each observation type (ranges and angles) such a correction function is derived from the project data. The parameters of these correction functions are determined simultaneously with the exterior orientation parameters (position and rotation) of the individual scans. All these parameters are determined during an adjustment such that the

vertical distance of scanned points to respective object planes are minimized. Consequently this method of on-the-job calibration requires a suitable number of planar regions on site. Such conditions can be fulfilled for example at manmade sites.

2. Theory and Method

We assume the following to be given: (i) several scans of the same scene obtained from different scan positions, and (ii) planar features included in the scene.

The method for detecting such planar features (termed patches in the following) is not scope of this paper. However, section 3.1. on the example data gives a short description of the method we applied.

2.1. Observations

The TLS usually delivers the scanned object points using Cartesian co-ordinates *x,y,z*. However, since the instrument originally performs polar measurements, these Cartesian co-ordinates should first be transformed to polar coordinates; see equation (1). The polar coordinates of the i^{th} measured point in the j^{th} scanner space are range, ρ_{ij}, horizontal direction, λ_{ij}, and elevation (vertical) angle, φ_{ij}. As a consequence of our aim – correction of measurements – three correction functions $\Delta\lambda$, $\Delta\varphi$ and $\Delta\rho$ are introduced in equation (1).

$$\lambda_{ij} = \arctan\left(\frac{y_{ij}}{x_{ij}}\right) + \Delta\lambda\left(\mathbf{x}^{\mathbf{AP}}\right), \quad \varphi_{ij} = \arctan\left(\frac{z_{ij}}{\sqrt{x_{ij}^2 + y_{ij}^2}}\right) + \Delta\varphi\left(\mathbf{x}^{\mathbf{AP}}\right) \tag{1.a,b}$$

$$\rho_{ij} = \sqrt{x_{ij}^2 + y_{ij}^2 + z_{ij}^2} + \Delta\rho\left(\mathbf{x}^{\mathbf{AP}}\right) \tag{1.c}$$

The actual form of the correction functions will be discussed in section 4.2. The parameters ($\mathbf{x}^{\mathbf{AP}}$) of these correction functions are called "additional parameters" (AP); e.g. by [2]. Others call them "calibration parameters" [7] or "interior orientation parameters".

2.2. Functional model

In the proposed algorithm, identical plane patches are observed from different scanner positions, so the parameters of the correction functions, the scanner orientation parameters and the patch parameters are adjusted simultaneously, with the condition that the measured points are on the patch.

The Cartesian coordinates of the observed range and angle measurements can be calculated using the inverse of equation (1).

$$\rho_{ij}, \lambda_{ij}, \varphi_{ij} \rightarrow x_{ij}, y_{ij}, z_{ij} \tag{2}$$

The Cartesian coordinates of this observed point are denoted as $\mathbf{p}_{ij}$. To convert these "scanner-based" coordinates to our global (project) coordinate system, the exterior orientation of the j^{th} scanner position is required. It consists of the rotation matrix, $\mathbf{M}_j$, and translation vector, $\mathbf{t}_j$. The point $\mathbf{p'}_{ij}$ in the global coordinate system is thus given by

$$\mathbf{p}'_{ij} = \mathbf{M}_j \cdot \mathbf{p}_{ij} + \mathbf{t}_j \tag{3}$$

The rotation matrix is constructed using the rotation angles around the three axes of the global coordinate system. [1] used quaternion representation for the rotations, but if the initial values

of these angles are close to the solution, classical rotation matrix representation is sufficient. The exterior orientation parameters of all scan positions are combined in the vector $\mathbf{x}^{\mathbf{EO}}$.

The parameters of the k^{th} patch in the global coordinate system are the plane normal $\mathbf{n}_k$ (with $\mathbf{n}_k^{\mathrm{T}} \cdot \mathbf{n}_k = 1$) and the patch constant m_k. The orthogonal distance d_{ijk} of the measured point, $\mathbf{p'}_{ij}$ from the k^{th} patch is:

$$d_{ijk} = \mathbf{p}'^{T}_{ij} \cdot \mathbf{n}_k - m_k \tag{4}$$

The parameters of all patches are combined and denoted as $\mathbf{x}^{\mathbf{pp}}$.

2.3. Stochastic model and formulation of the adjustment

Our aim is to determine the additional parameters ($\mathbf{x}^{\mathbf{AP}}$), the exterior orientation ($\mathbf{x}^{\mathbf{EO}}$) and the patch parameters ($\mathbf{x}^{\mathbf{PP}}$) such that all observed points $\mathbf{p'}_{ij}$ lie as close as possible to their respective patch plane. For doing this simultaneously we apply a least squares adjustment based on equation (4). Since $\mathbf{p'}_{ij}$ in equation (4) is a function of the original polar measurements (ρ, φ, λ), such a least squares adjustment requires a Gauss-Helmert model minimizing the residuals of these original polar measurements. As the normal vectors of the patch parameters must be normalized, this constraint needs to be included in the adjustment process.

The formulation in the Gauss-Helmert model leads to the following system of equations:

$$\begin{aligned} &\text{Conditions (points on planes):} && \underset{(h,n)}{\mathbf{B}}\,\underset{(n,1)}{\mathbf{v}} + \underset{(h,r)}{\mathbf{A}}\,\underset{(r,1)}{\mathbf{x}} - \underset{(h,1)}{\mathbf{l}} = \underset{(h,1)}{\mathbf{0}} \\ &\text{Constraints (length of normal vectors):} && \underset{(p,r)}{\mathbf{C}}\,\underset{(r,1)}{\mathbf{x}} - \underset{(p,1)}{\mathbf{w}} = \underset{(p,1)}{\mathbf{0}} \end{aligned} \tag{5}$$

B: Jacobian of the conditions (equation 4.) with respect to the observations
A: Jacobian of the conditions (equation 4.) with respect to the unknown parameters
C: Jacobian of the constraints ($\mathbf{n}_k^{\mathrm{T}} \cdot \mathbf{n}_k = 1$) with respect to the unknown parameters
v: vector of residuals of the observations
x: vector of corrections to unknown parameters ($\mathbf{x}^{\mathbf{AP}}$, $\mathbf{x}^{\mathbf{EO}}$ and $\mathbf{x}^{\mathbf{PP}}$)
l: is the misclosure vector of the conditions
w: is the misclosure vector of the constraints
n: is the number of observations (i.e. three times the number of observed points)
h: is the number of condition equations (i.e. the number of points)
r: is the number of unknown parameters
p: is the number of constrains (i.e. the number of planes)

Using the "constrained minima" method [8] the cost function Φ to be minimized is given by:

$$\Phi = \underset{(1,n)}{\mathbf{v}^T}\,\underset{(n,n)}{\mathbf{P}}\,\underset{(n,1)}{\mathbf{v}} - 2\,\underset{(1,h)}{\mathbf{k}_1^T}\left(\underset{(h,n)}{\mathbf{B}}\,\underset{(n,1)}{\mathbf{v}} + \underset{(h,r)}{\mathbf{A}}\,\underset{(r,1)}{\mathbf{x}} - \underset{(h,1)}{\mathbf{l}}\right) - 2\,\underset{(1,p)}{\mathbf{k}_2^T}\left(\underset{(p,r)}{\mathbf{C}}\,\underset{(r,1)}{\mathbf{x}} - \underset{(p,1)}{\mathbf{w}}\right) \tag{6}$$

where $\mathbf{k_1}$ and $\mathbf{k_2}$ are Lagrange multiplier vectors. The **P** matrix is the weight matrix of the observations. In the case of uncorrelated observations it is a diagonal matrix, and the diagonal elements are the inverses of the squares of the *a priori* standard deviations of the observations (σ_ρ , σ_φ , σ_λ), which may be obtained from the technical specification of the TLS used.

After computing the partial derivatives of Φ with respect to **v**, **x**, $\mathbf{k_1}$ and $\mathbf{k_2}$, and substituting $\mathbf{k_1}$ by **x**

$$\underset{(h,1)}{\mathbf{k_1}} = \left(\underset{(h,n)}{\mathbf{B}^T} \underset{(n,n)}{\mathbf{P}^{-1}} \underset{(n,h)}{\mathbf{B}} \right)^{-1} \left[\underset{(h,1)}{\mathbf{l}} - \underset{(h,r)(r,1)}{\mathbf{A}\,\mathbf{x}} \right] = \underset{(h,h)}{\mathbf{N}}^{-1} \left(\underset{(h,1)}{\mathbf{l}} - \underset{(h,r)(r,1)}{\mathbf{A}\,\mathbf{x}} \right) \tag{10}$$

we get the following system of equations:

$$\begin{bmatrix} -\underbrace{\left(\mathbf{A}^T\mathbf{N}^{-1}\mathbf{A}\right)}_{(r,r)} & \underset{(r,p)}{\mathbf{C}} \\ \underset{(p,r)}{\mathbf{C}^T} & \underset{(p,p)}{\mathbf{0}} \end{bmatrix} \begin{bmatrix} \underset{(r,1)}{\mathbf{x}} \\ \underset{(p,1)}{\mathbf{k_2}} \end{bmatrix} = \begin{bmatrix} -\underbrace{\mathbf{A}^{\mathbf{T}}\mathbf{N}^{-1}\mathbf{l}}_{(r,1)} \\ \underset{(p,1)}{\mathbf{w}} \end{bmatrix}. \tag{11}$$

The solution of this system yields $\mathbf{x}$, which then gives $\mathbf{k_1}$, using equation (10). The residuals can then be computed by

$$\underset{(n,1)}{\mathbf{v}} = \underset{(n,n)}{\mathbf{P}^{-1}} \underset{(n,h)}{\mathbf{B}} \underset{(h,1)}{\mathbf{k_1}} \tag{12}$$

3. Data

For testing the on-the-job calibration we used two scans of a room, acquired from two different scanner positions. The length, width and height of the room were 6.3 m, 3.4 m and 2.4 meters respectively. The first scanner position (SP1) was almost in the middle of the room, the second (SP2) was 0.9 m away from the shorter, and 1.4 m away from the longer wall. The scanner height from the floor was approximately 1.2 m in both scanner positions.

The data acquisition was made with a *Faro Photon* laser scanner. Originally ca. 10 million points in total were measured. For our investigations we used a subset by selecting of ca. 20.000 points in total. The instrument has better performance, than the *Faro LS880* instrument investigated previously by the authors [9]. The *internal* calibration (compensation – in Faro nomenclature) applied by the controlling software *FaroScene* on scanned data was also significantly modified by the manufacturer compared to the previous internal calibration.

For the investigated scanner, the non-periodic internal calibration function defined by a look-up table was omitted. Nevertheless, it fulfils a systematic range error of less than 2 mm up to 25 m, as stated within the instrument's specification. According to our results, the current internal calibration applies the short periodic calibration differently, compared to the former version. While the wavelength of the short periodic calibration function appears similar to the previous (60cm), the amplitude seems to be a function of the measured intensity. So the actual meaning of the intensity based distance correction function has significantly changed, as it is not simply an addition to the measured distance, but it has an effect on the amplitude of the short periodic harmonic correction function. As we currently have no further information from the manufacturer, we could not find out the actual form of this method.

For some experiments we disabled the internal calibration parameters described here and we refer it as ‘turning off internal calibration’.

3.1. Patch determination

As the room had a very simple rectangular geometry, we used a simple patch determination method. The room had six segments (almost planar surfaces): four walls, the ceiling and the floor. We defined a ‘project’ coordinate system, centered on a lower corner of the room, and

the axes of this coordinate system were parallel to the edges of the room, with an accuracy of 2-4cm. We manually selected rectangular polygons on walls, floor and ceiling, that were not affected by artificial objects e.g. light switch or stucco paintings. We defined these polygons by the 3D coordinates of the corner points. Then we parceled these polygons to rectangles with fixed patch size, and selected from the scanner dataset the point belonging to the patches using bounding boxes. For the first experiments we used a patch size of 1.2 m. Afterwards experiments were conducted with reducing this patch size.

4. Results

We made several adjustments to determine the exterior orientation of the two scans and the patch parameters. Additionally, we processed without and with on-the-job calibration. In the latter case, we investigated the effects that occur if internal calibration is turned on or off, the effects of different patch sizes, and the effect of different correction functions.

4.1. Results without on-the-job calibration

At first only the internal calibration was used and no on-the-job calibration was computed. Then one scan was triangulated and the normal distances of the points of the second scan were determined. The color codings of these normal distances are shown in figure 1 (left). The scanner data fulfills the precision criteria claimed by Faro. Nevertheless remaining systematic errors can be seen. Consequently the applied internal calibration does not sufficiently eliminate all the systematic measurement errors. If the internal calibration is turned off before computing the adjustment (without on-the-job calibration) then the remaining normal distances between both scans are shown in figure 1 (right). The distribution of these residual systematic errors is different, however the size of the errors are quite similar.

Therefore we set out to eliminate the systematic errors by on-the-job calibration. In order not to compensate effects of a probably insufficient internal calibration (especially considering the intensity based part) and to work with data that is as unmodified as possible, we turned the internal calibration off for the following experiments with on-the-job calibration.

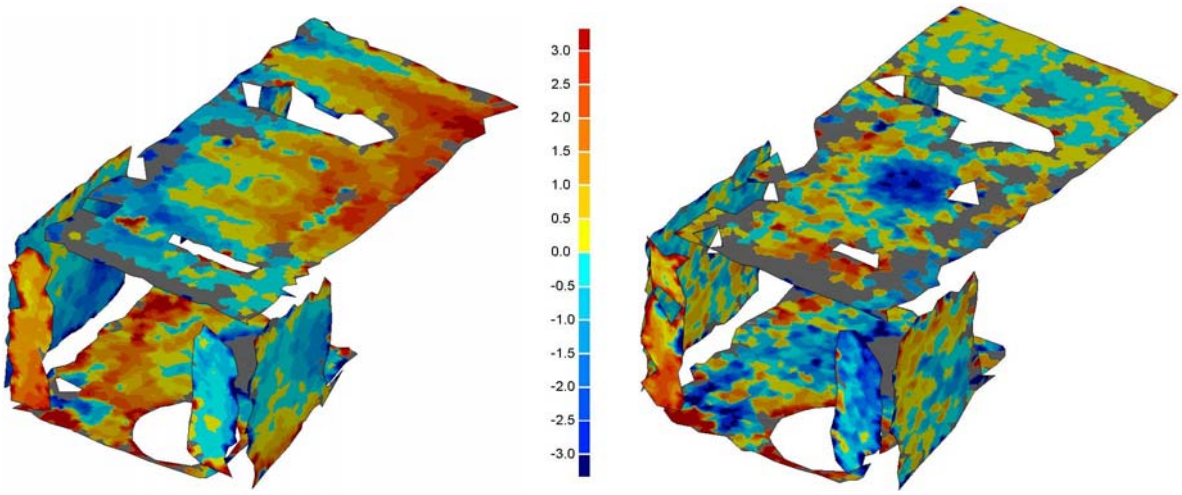

Figure 1: Left: Difference between both scans (normal distances between triangulation of scan 1 and the points of scan 2) (Faro internal calibration turned on). Right: The same without internal calibration. The RMS values of the normal differences of the points of both scans to their respective adjusted patch planes are 2.8mm (internal calibration turned on) and 1.67mm (internal calibration turned off) respectively.

4.2. The range and angular correction functions

In our previous paper, [9] we applied a piecewise linear range correction function. The advantage of that function was that it required no assumption on the shape of the range calibration function. However, in order to achieve short periodic corrections short interval lengths are required, which consequently raises the number of unknown parameters. In this paper we try a different calibration function, which is the sum of a piecewise linear and a harmonic function. The advantage of this combined function is that it unifies the advantages of harmonic functions as 'smooth' functions for short periodic errors, and the freeform of piecewise linear function for non-periodic errors.

For our calculations, we defined a "basic wavelength". For periodic part of the calibration function we estimated the coefficient for sinus and cosine functions with the basic wavelength, the half, third and fourth of it. For piecewise linear part of the calibration function we used this basic wavelength as the range interval for range sections. Thus the range correction has the following form:

$$\Delta\rho(\rho) = \boldsymbol{a}_i + \frac{\boldsymbol{a}_{i+1} - \boldsymbol{a}_i}{\delta\rho} \cdot (\rho - \rho_i) + \sum_{j=1}^{4} \left(\boldsymbol{d}_{j0} \cdot \sin\left(\frac{2\pi \cdot \rho}{\delta\rho \cdot \boldsymbol{j}} \right) + \boldsymbol{d}_{j1} \cdot \cos\left(\frac{2\pi \cdot \rho}{\delta\rho \cdot \boldsymbol{j}} \right) \right) \tag{13}$$

if: $\rho_i \le \rho < \rho_{i+1}$ with i = 1,…, M+1. The basic wavelength is $\delta\rho = \rho_{i+1} - \rho_i$ .The $\boldsymbol{a}$-s are the coefficients of the piecewise linear function, and $\boldsymbol{d}$-s are the coefficients of harmonic function.

For correcting the vertical angles we used the very same form also as a correction function, but now as a function of the vertical angle. (Originally also a correction function for the horizontal angles was used, but it turned out that it did not improve the results significantly.)

We investigated the effect on the differences between the two scans if only the ranges, only the vertical angles and both (ranges and vertical angles) are corrected; see figure 2. From there we can see that already the correction of only one type of measurement achieves practically the same result as correcting both.

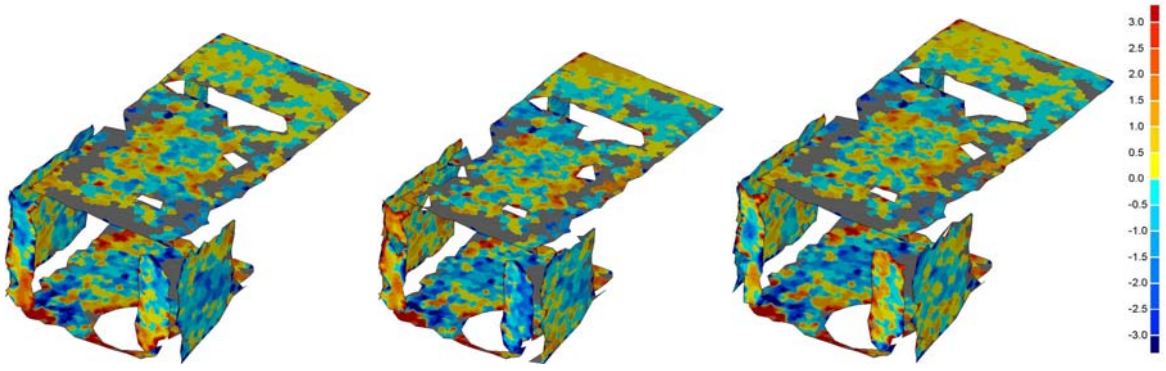

Figure 2. Difference between both scans (normal distances between triangulation of scan 1 and the points of scan 2) Left: correcting only ranges; Centre: correcting only vertical angles; Right: correcting both; the respective RMS values of the normal differences of the points of both scans to their respective adjusted patch planes are 1.29mm (only ranges), 1.27mm (only vertical angles) and 1.24mm (both).

4.3. Range correction function with different short periodic wavelengths

In another experiment we computed the range calibration function with different basic wavelengths 10cm, 20cm, 30cm and 40cm. Fig 3. shows the obtained range calibration functions.

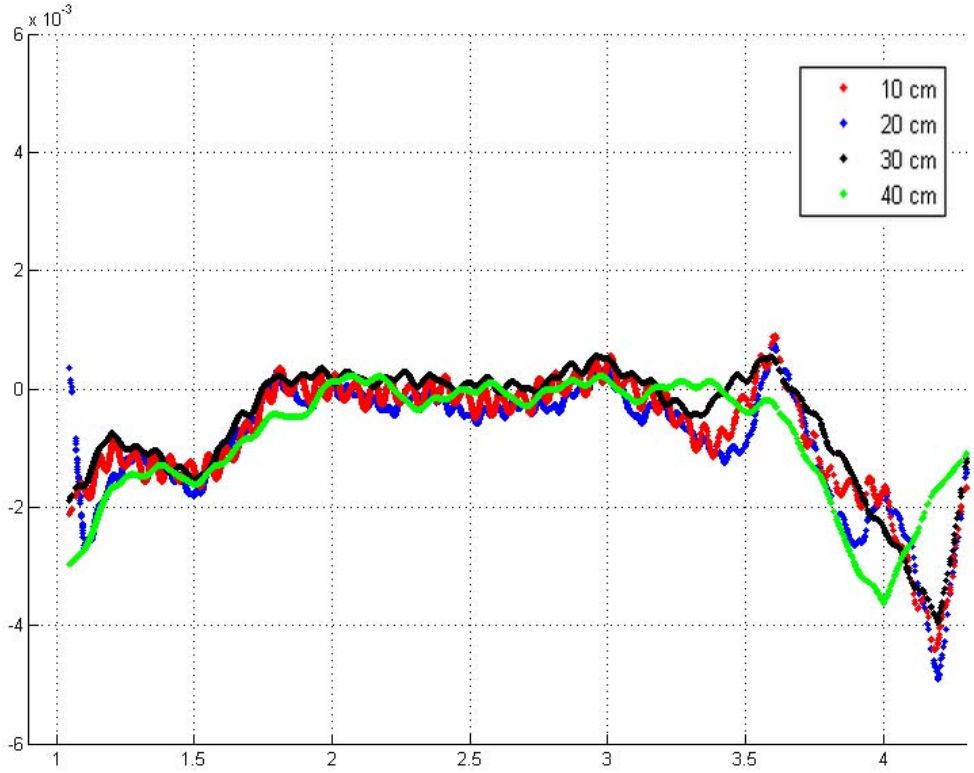

Figure 3: Range correction function with varying basic wave length (40cm to 10cm), for 1.2 meter patchsize. For this experiment the internal calibration was turned off. The 1.5-3.3 meter range interval has enough number of points to get a stable solution for the range correction function. Range intervals outside this range interval have less points, and so have less effect on the form of the calibration function.

Although the different range correction functions show for some ranges range correction values, which differ between 0.5mm and 1mm, the effect on the remaining differences between both scans is negligible; see Fig 4. Consequently the choice of the basic wave length (for the data in this experiment) appears only of limited importance.

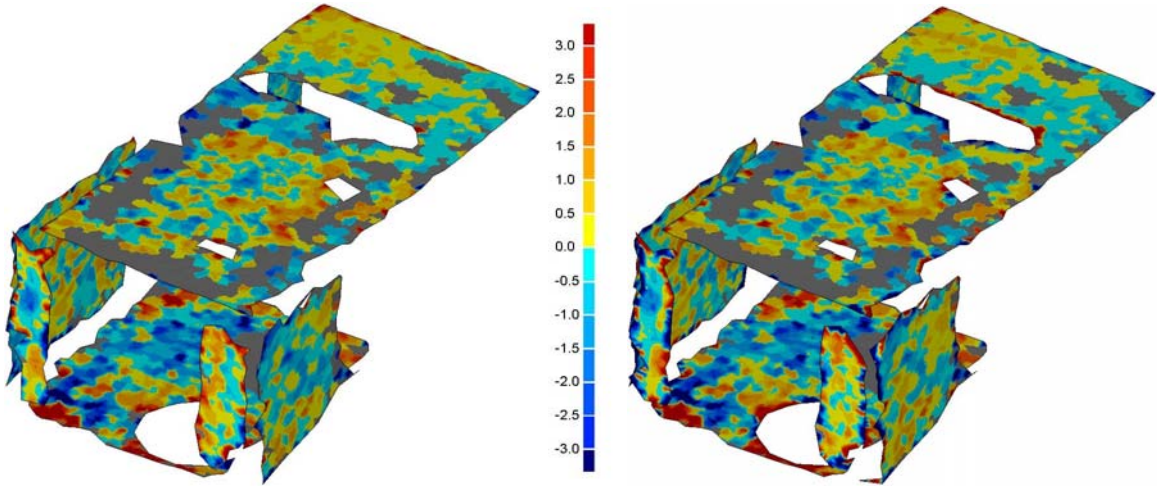

Figure 4: Difference between both scans (normal distances between triangulation of scan 1 and the points of scan 2), patch size 1,2 meter. Left: Basic wavelength: 40cm, Right: 10cm.

4.4. The effect of patch size on range correction function

Finally we computed the range correction function with different patch sizes; see figure 5. From this figure we see that with decreasing the patch sizes also the correction functions tend to become unstable.

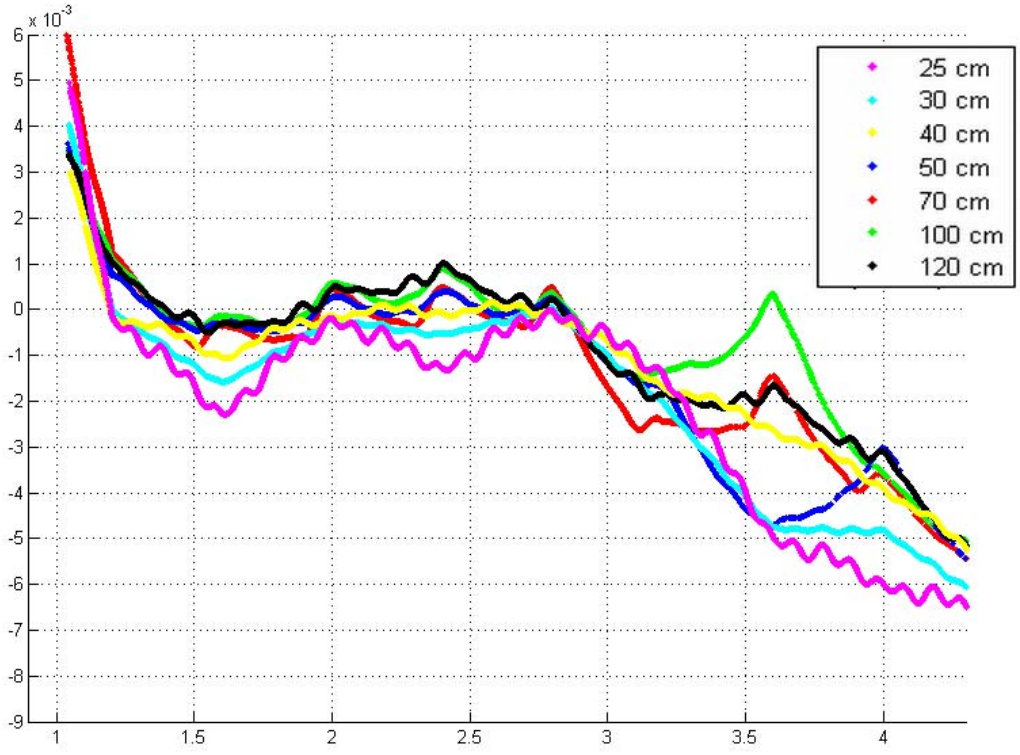

Figure 5. Different range correction functions for datasets (internal calibration turned off). Basis wavelength of range calibration function was 0.4m. Patch size ranged from 0.25m to 1.2m. For the ranges larger than 3.5m and below 1m the calibration functions show larger differences.

5. Discussion

In this work we presented a rigorous approach for simultaneously determining the exterior orientation of scan positions and on-the-job calibration parameters (both for range and angles) together with object planes. This approach therefore requires a suitable number of planar patches to be available at the object. The number of patches and thus the adaptability to a certain non-planarity of the object is controlled by the patch size. This approach has the benefit of utilizing the large point density of todays terrestrial scanners and the large overdetermination that follows with it. The adjustment is formulated following the Gauss-Helmert model.

The correction functions for the on-the-job calibration used in this work are a sum of a periodic and a piecewise linear function. The number of unknown correction parameters for it is controlled by selecting a basic wave length.

The experiments with the example data showed that an improvement of the original status of the data is possible. The RMS of the normal distances of the points of the scans to the adjusted patches decreased from 1.7mm to 1.2mm. These RMS values contain the noise of the data, systematic errors still remaining after the on-the-job calibration, but also any deviations of the object from planarity.

Experiments which corrected only the ranges, only the vertical angles, or both did not show significantly different RMS values. We conclude, that the setup of our experiment (i.e. the positions and rotations of the scans and geometry of the object) does not allow a unique identification of the real causes of the systematic patterns visible in the original status. Here the setup was: two scans close to each other with same height and rotation and a simple room geometry (with some walls only partially covered by data). This led to a high correlation between the distribution of the angles and the measured ranges; e.g. the angular area around zenith direction had similar ranges for both scans.

Further experiments (during which the patch size and the basic wave length were varied) produced different range correction functions. The effects on the object were, however, similar. Consequently from the current experiment we can not give a recommendation on the best choice of these parameters.

We therefore conclude that very small patch sizes and very flexible correction function (i.e. with many unknowns) are not optimal for scanning configurations used in practical approaches today. Nonetheless an improvement was possible with any choice of correction functions. In the future, we want to investigate two possible solutions: a) adapting the scanning configuration (similar to the synthetic experiments in [10]) in order to de-correlate the measurements, and b) to reduce the number of unknown correction parameters.

Acknowledgements

This work was supported by *Schloß Schönbrunn Kultur und Betriebsges.m.b.H.* and by *Steinmetzbetriebe Franz Bamberger* and funded by the *Christian Doppler Research Association*.

References:

[1] Gielsdorf, F., Rietdorf, A. & Gruendig, L., 2004: A Concept for the calibration of terrestrial laser scanners. – Proceedings FIG Working Week, Athens, Greece, on CD-ROM.

[2] Lichti, D. D., 2007: Error modeling, calibration and analysis of an AM-CW terrestrial laser scanner system. – ISPRS Journal of Photogrammetry and Remote Sensing 61 (5): 307-324.

[3] Kersten, Th., Mechelke, K., Lindstaedt, M. & Sternbernberg, H., 2008: Geometric Accuracy Inves-tigations of Latest Terrestrial Laser Scanning Systems. – Proceedings FIG Working Week, Stock-holm, Sweden, on CD-ROM.

[4] Pfeifer N., Dorninger P., Haring A., Fan H.: Investigating terrestrial laser scanning intensity data: quality and functional relations. 8th Conference on Optical 3-D Measurement Techniques, pp. 328 - 337, Zurich, Switzerland, 2007.

[5] Amiri Parian, J. & Gruen, A., 2005: Integrated laser scanner and intensity image calibration and accuracy assessment. – The International Archives of the Photogrammetry, Remote Sensing and Spatial Information Sciences 36 (3/W19):18-23.

[6] Schneider, D. & Maas, H.-G., 2007: Integrated bundle adjustment with variance component estimation – fusion of terrestrial laser scanner data, panoramic and central perspective image data. – The International Archives of the Photogrammetry, Remote Sensing and Spatial Information Sciences 36

[7] Ingensand, H., Ryf A. & Schulz T., 2003: Performances and Experiences in Terrestrial Laserscanning. – Proceedings of the 6th Conference on Optical 3D Measurement Techniques, Zurich, Switzerland.

[8] Mikhail, E. M., 1976: Observations and Least Squares. IEP – a Dun-Donnelley Publisher, New York. 497 pp.

[9] Molnár G., Pfeifer N., Ressl C., Dorninger P. and Nothegger C.: Range calibration of terrestrial laser scanners with piecewise linear functions. Photogrammetrie, Fernerkundung, Geoinformation, 2009(1), pp. 563-576, 2009.

[10] Bae, K. H., & Lichti, D. D., 2007: On-site self-calibration using planar features for terrestrial laser scanners. – The International Archives of the Photogrammetry, Remote Sensing and Spatial Informa-tion Sciences 36 (3/W52): 14-19.